International Journal of Engineering Research & Technology (IJERT)
ISSN: 2278-0181
Vol. 3 Issue 7, July - 2014

Cause and Effect of Tellurium Precipitates on $Cd_{1-X}zn_xte$ Thin Film Formation

Dr. Monisha Chakraborty
Assistant Professor, School of Bio-Science & Engineering,
Jadavpur University,
Kolkata-700032, India

Sugata Bhattacharyya
Project Fellow, School of Bio-Science & Engineering,
Jadavpur University,
Kolkata-700032, India

Abstract--In this work, an increased Tellurium precipitation along with an improved formation of $Cd_{1-x}Zn_xTe$ compound from individual layer-deposited CdTe and ZnTe thin films by a single R.F. Magnetron Sputtering unit under various annealing environments are observed. The number and intensity of the Tellurium planes increased in the XRD data from the Nitrogen to Argon to vaccum Annealing. Tellurium precipitation also kept a correspondence with the number and intensities of the formed $Cd_{1-x}Zn_xTe$ planes and the increased inertness of the respective annealing-ambience. The increased Tellurium precipitation also ensured a respective change in the transmittance property of the films, particularly in near band-gap-region of Tellurium. It also enhanced the films photoluminescence intensity correspondingly from the Nitrogen to the vaccum-annealed samples. In that context, the increased ionized donor bound excitons, a function of the Tellurium precipitate, and that of the neutral donor bound excitons has led to a relative increase of the PL intensity from the Nitrogen to the vaccum-annealed samples. A selective formation of 220 $Cd_{1-x}Zn_xTe$ planes, as opposed to 111 and 311 planes, is also observed in Nitrogen-annealed sample than in vaccum or Argon-annealed sample.

Keywords--Annealing, Tellurium Precipitation, $Cd_{1-x}Zn_xTe$, Thin Film, Single R.F. Sputtering

1. INTRODUCTION

In recent times, CdZnTe (CZT) has developed a significant region of interest in the fields of medical imaging, Computed Tomography (CT), Single Photon Emission Computed Tomography (SPECT), Integration-Mode X-Ray Radiography, Photon-Counting, Surgical-Oncology, Positron Emission Tomography (PET) [1] and Dedicated Emission Mammotomography [2]. This ternary semiconductor alloy too has found prominence as a device-grade material for room-temperature nuclear radiation detectors, substrate for IR-detector material like HgCdTe, light emitting diodes and solar-cells [3-10]. With its band-gap lying between 1.45-2.25 eV [11], the variation of the either Cd or Zn content can manipulate the band-gap of CdZnTe. Large scale fabrication like batch-production of CdZnTe thin-film on medium to large substrate areas can be implemented by Sputtering. The selected stoichiometry of $Cd_{1-x}Zn_xTe$ or rather the value of 'x', can be easily controlled by using a co-sputtering machine with respective

CdTe and ZnTe targets [12] or ZnTe and Cd [13] targets or vice-versa. But in case of less-equipped laboratories or rather in case of lack of Co-Sputtering machine, $Cd_{1-x}Zn_xTe$ thin films can be created by means of individual layer deposition of CdTe and ZnTe films, one above the other, respectively.

. $Cd_{1-x}Zn_xTe$ can be formed from the consecutive layers of CdTe and ZnTe thin films. In that regard, the formation of $Cd_{1-x}Zn_xTe$ compound is largely accompanied by high Tellurium precipitation. In our work, our objective has been to study the opto-structural impact of this associated Tellurium precipitation and its corresponding relation regarding with the formation of $Cd_{1-x}Zn_xTe$ compound, in case of layer by layer deposition of CdTe and ZnTe thin films from a Single R.F. Magnetron Sputtering Unit.

2. EXPERIMENTAL PROCEDURE

A single 75mm × 25mm × 1.3 mm of glass slide was used as a substrate for thin film preparation. The glass slide was initially weighed and then was cleansed in acetone for 25 minutes, inside a glass-container. The glass-container was placed in a distill-water environment. "Piezo-Ultrasonic Cleaner" was used for the above cleansing process.. The "Planar Magnetron Sputtering Unit", with Model No.: 12"MSPT, was used to deposit the consecutive CdTe and ZnTe layers on the glass substrate. For both the deposition, substrate-heating was carried out at 200℃. Substrate-heating was started at a chamber pressure of 10^{-3} mBar. At a chamber-pressure of 10^{-4} mBar, Argon was entered for sputtering. The line pressure of Argon was maintained at 1.26 Kg/cm^2. During the Sputtering process chamber-pressure was kept constant at 0.035 mBar. The Sputtering- Forward Power was maintained at 410 Watt and the Reflected Power at 50 Watt. The required stoichiometry of the proposed $Cd_{1-x}Zn_xTe$ film was obtained by controlling the "deposition-time" of the CdTe and ZnTe sputter-targets. The CdTe layer is deposited first and then the ZnTe layer is deposited above it. On

completion of Sputtering, the substrate was allowed to cool off on its own. The Diffusion pump was kept on till the substrate-temperature reached 50℃, in order to avoid any form of oxidation. The air-admittance valve was opened only after the substrate has reached room-temperature. The glass slide, with bi-layered CdTe and ZnTe thin films on it, was ultimately cut into 4 pieces with dimensions of 18mm ✕ 25mm × 1.3 mm each. The three out of the four cut-pieces were respectively subjected to vaccum, Nitrogen and Argon-annealing for 1 hour each. Annealing was carried out in the same sputter-machine, at a temperature of 200 ℃. The temperature was manually maintained at the aforesaid value with an error of ± 2℃. In case of Argon and Nitrogen-Annealing, the concerned gases were entered at line-pressure of 1.26 Kg/cm^2. The chamber-pressure during Argon and Nitrogen-annealing was kept at 0.035 mBar. During vaccum-annealing, the same chamber pressure was in between 10^{-4}-10^{-5} mBar. The fourth cut-piece was left un-annealed.

3. THEORY AND CALCULATION

The combined CdTe and ZnTe thin film thickness were decided to be 350 nm. The value of 'x' in the $Cd_{1-x}Zn_xTe$ was considered to be '0.35'. The projected model for finding the thickness of CdTe and ZnTe based on the value of 'x' is as follows [14]:

$$\frac{x}{1-x} = \frac{n_{ZnTe}}{n_{CdTe}}$$

or,

$$\frac{x}{1-x} = \frac{\frac{m_{ZnTe}}{M_{ZnTe}}}{\frac{m_{CdTe}}{M_{CdTe}}} \quad \ldots\ldots\ldots (1)$$

Where,

n_{ZnTe} = No. of moles of ZnTe

m_{ZnTe} = deposited mass of ZnTe

M_{ZnTe} = Molar-Mass of ZnTe

n_{CdTe} = No. of moles of CdTe

m_{CdTe} = deposited mass of CdTe

M_{CdTe} = Molar-Mass of CdTe

or,

$$\frac{x}{1-x} = \frac{m_{ZnTe}}{m_{CdTe}} \times \frac{M_{CdTe}}{M_{ZnTe}}$$

or,

$$\frac{x}{1-x} = \frac{\delta_{ZnTe} \times A \times h_{ZnTe}}{\delta_{CdTe} \times A \times h_{CdTe}} \times \frac{M_{CdTe}}{M_{ZnTe}} \quad \ldots\ldots\ldots (2)$$

Where,

δ_{ZnTe} = density of ZnTe

h_{ZnTe} = Height of Deposited Film of ZnTe

δ_{CdTe} = density of CdTe

h_{CdTe} = Height of Deposited Film of CdTe

$\therefore$, ,

$$\frac{x}{1-x} = \frac{\delta_{ZnTe} \times h_{ZnTe}}{\delta_{CdTe} \times h_{CdTe}} \times \frac{M_{CdTe}}{M_{ZnTe}}$$

For, x = 0.35, then $1-x$ = 0.65

And,

$$\delta_{ZnTe} = 6.34 gm/cm^3$$
$$\delta_{CdTe} = 5.85 gm/cm^3$$
$$M_{ZnTe} = 193 gm/mol$$

$$M_{ZnTe} = 240 gm/mol$$

We get,

h_{ZnTe} = 133.6592 nm

h_{CdTe} = 216.3408 nm

By using the formulae

$$mass\ difference = h \times \rho_{CdTe} \times A$$

&

$$mass\ difference = h \times \rho_{ZnTe} \times A,$$

Where,

ρ_{CdTe} = density of CdTe and ρ_{ZnTe} = density of ZnTe, 'A' is the surface area of the glass slides

The values of the thicknesses were found. Thickness of CdTe and ZnTe were found to be 216.1022 nm and 133.8348 nm respectively, by subtracting the initial actual glass-slide weight from the film deposited glass-slide weight. The total thickness of the bi-layered thin film experimentally thus found to be 349.937 nm.

From the new experimentally obtained thickness values of CdTe and ZnTe, the values of 'x' and '1-x' became 0.3505 and 0.6495 respectively.

4. RESULTS AND DISCUSSIONS

4.1 X-Ray Diffraction (XRD) Results

Rigaku Minifleax powder diffractometer was used to determine the X-Ray Diffraction spectra of all the films. X-ray emissions from Copper-Kα lines were of the wavelength of 1.54025Å. 4 different types of $Cd_{1-x}Zn_xTe$ planes were observed in the XRD spectra of the vaccum, Argon and Nitrogen-annealed samples. The Un-Annealed sample revealed no such $Cd_{1-x}Zn_xTe$ planes. Both the vaccum and Argon-annealed samples revealed the planes with Miller Indices 111, 311 and 400 respectively. The Nitrogen-annealed sample only revealed the 220 and 400 planes. All the observed $Cd_{1-x}Zn_xTe$ planes were found to lie in between the standard 111, 220, 311 and 400 planes of cubic-CdTe and cubic-ZnTe crystallography. Standard JCPDS files 150770/752086 and 150746/800022 provides

the XRD data of standard cubic-CdTe and cubic-ZnTe crystallography respectively. So the observed $Cd_{1-x}Zn_xTe$ planes in our samples can possibly be of cubic-crystallography. Also the standard $Cd_{0.78}Zn_{0.22}Te$ planes of JCPDS file No. 471296 is of rhombohedral-crystallography. The 003, 220, 401 and 404 planes of standard $Cd_{0.78}Zn_{0.22}Te$ lie in the same 2θ region of the observed $Cd_{1-x}Zn_xTe$ planes of our samples. This is shown in detail in Table 5. So the above standard planes of rhombohedral crystallography represent the one and the same 111, 220, 311 and 400 planes of cubic-crystallography. Since rhombohedral–crystallography is very much similar to that of cubic-crystallography, with all the three edges and in-between angles (α) being equal in both the structure, the observed $Cd_{1-x}Zn_xTe$ peaks can be very much of cubic or rhombohedral-crystallography. Also in the standard JCPDS file the $Cd_{0.78}Zn_{0.22}Te$ planes with rhombohedral crystallography had an angle α=89.94° i.e. ~90°. Hence the sanctity of the observed $Cd_{1-x}Zn_xTe$ peaks is unambiguous. The selective formation of the 220 CZT plane in case of Nitrogen annealed sample is interesting to note. The 220 plane in case of the Nitrogen annealed sample occurs without the bordering 111 and 311 planes. In case of cubic CdTe and ZnTe, the 220 plane formation also occurs directly in between the 111 and 311 planes. Thus it is highly possible here that under the Nitrogen-annealing environment, the 220 plane of $Cd_{1-x}Zn_xTe$ has grown at the cost of the 111 and 311 planes. Secondly an increased Tellurium precipitation is observed in all the annealed-samples with a direct proportionality of its intensities being maintained with the intensities and the number of the formed $Cd_{1-x}Zn_xTe$ peaks. It is mostly because of the fact that the increased bonding of the Cadmium ions with ZnTe crystals takes place in the more inert annealing environments, correspondingly causing a better formation of $Cd_{1-x}Zn_xTe$ peaks and increased Tellurium precipitation and more Cadmium vacancies. Table 6 represents the lattice-constants of the observed $Cd_{1-x}Zn_xTe$ planes corresponding to cubic-crystallography. Here an increased value of lattice constant of the CZT compounds from vaccum to Argon to Nitrogen-annealing is observed. It implies an increased value of Zinc-content in the CZT compound has occurred, as the lattice constant has shifted more from the CdTe side to the ZnTe side. The above fact indicates that though increased Cadmium ion bonding takes place in case of vaccum annealed samples and decreases towards the Nitrogen-annealed side, the covalent cadmium bonds formed with the ZnTe crystals in CZT compounds are weaker compared to that of the general CdTe and ZnTe bonds. So, these CZT bonds are more quickly broken and are facilitated by the evaporation of Cadmium from the sample surface because of the high heating time. It thus can be concluded that though better bonding of Cd ions to ZnTe crystals takes place in case of increasing inertness of the annealing-environment i.e. from Nitrogen to vaccum, the higher heating time and the weaker CZT bonds leads to an increasing Cadmium evaporation from the CZT compounds. This trend of breaking of covalent Cadmium-bonds from CZT increases with increasing inertness of the annealing environment. Thus increased Zinc content and a corresponding higher lattice constant of the formed CZT is observed from the vaccum to the Nitrogen-annealed sample. The un-annealed sample showed no such peaks of $Cd_{1-x}Zn_xTe$ as expected. Figure 1, 2, 3 and 4 show XRD spectra of the vaccum, Argon, Nitrogen and un-annealed samples. The Tables 1, 2, 3 and 4 provide the individual description of the peaks observed in XRD spectra of the vaccum, Argon, Nitrogen and un-annealed samples. Table 5 gives a detailed analysis of the observed of $Cd_{1-x}Zn_xTe$ planes from the vaccum to Nitrogen-annealed samples, in situ with their relation to the standard JCPDS Cubic-CdTe and ZnTe file and the standard JCPDS Cd0.78Zn0.22Te file. The Table 6 supplies the information about the lattice-constants of the observed $Cd_{1-x}Zn_xTe$ planes in all the annealed samples, considering a cubic crystallography, using the equation $a = d(h^2 + k^2 + l^2)^{1/2}$. Here'd' is the inter-planar distance between the corresponding planes, with a Miller index values of hkl.

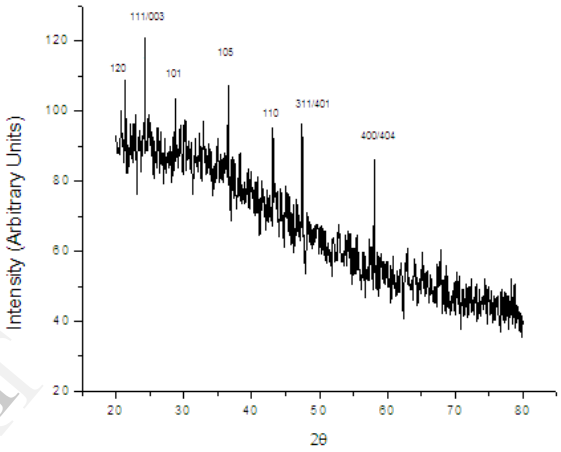

Fig 1: XRD of Vaccum-Annealed Sample

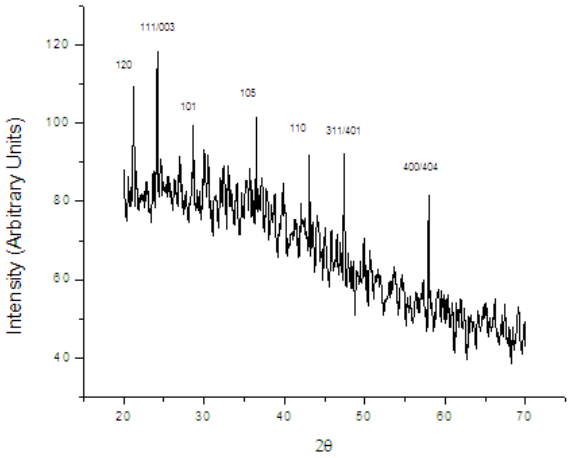

Fig 2: XRD of Argon-Annealed Sample

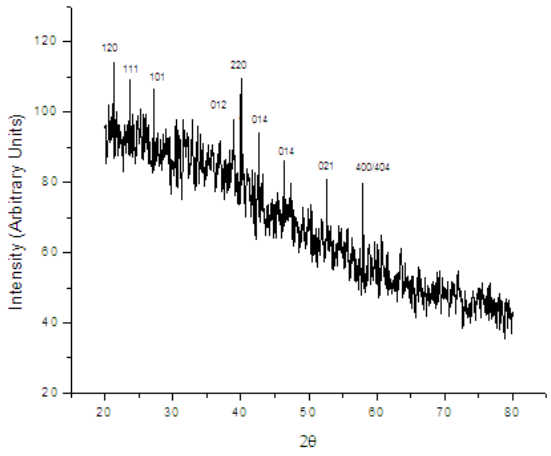

Fig3: XRD of Nitrogen-Annealed Sample

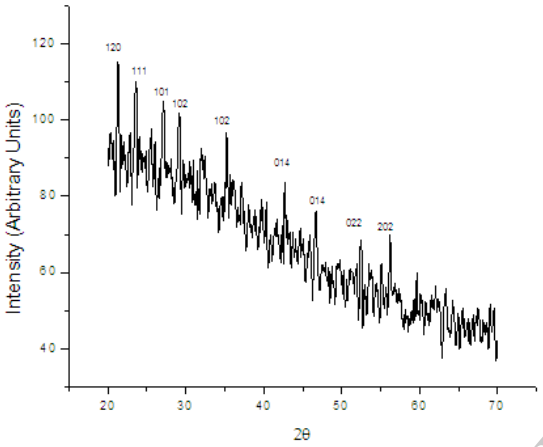

Fig 4: XRD of Un-Annealed Sample

Table 1: Vaccum-Annealed Sample

Observed Angle (Degree)	Compound/Element	Observed Intensity (I/Io)	Observed Plane	Crystal Structure	JCPDS File No.
21.35	CdTe	89.90827	120	Orthorhombic	410941
24.26	CdZnTe	100	111/003	Cubic/ Rhomboh edral	471296 (Rhomb ohedral)
28.73	Te	85.59631	101	Hexagonal	850563
36.53	Te	88.71563	105	Hexagonal	011313
43.13	Te	78.53215	110	Hexagonal	850563
47.45	CdZnTe	79.63307	311/401	Cubic/ Rhomboh edral	471296 (Rhomb ohedral)
58.07	CdZnTe	71.19267	400/404	Cubic/ Rhomboh edral	471296 (Rhomb ohedral)

Table 2: Argon-Annealed Sample

Observed Angle (Degree)	Compound/Element	Observed Intensity (I/Io)	Observed Plane	Crystal Structure	JCPDS File No.
21.3	CdTe	92.29043	120	Orthorhombic	410941
24.25	CdZnTe	100	111/003	Cubic/ Rhomboh edral	471296 (Rhomb ohedral)
28.7	Te	83.84917	101	Hexagonal	850563
36.5	Te	85.70624	105	Hexagonal	011313
43.15	Te	77.43387	110	Hexagonal	850563
47.4	CdZnTe	77.94034	311/401	Cubic/ Rhomboh edral	471296 (Rhomb ohedral)
58	CdZnTe	68.82386	400/404	Cubic/ Rhomboh edral	471296 (Rhomb ohedral)

Table 3: Nitrogen-Annealed Sample

Observed Angle (Degree)	Compound/ Element	Observed Intensity (I/Io)	Observed Plane	Crystal Structure	JCPDS File No.
21.29	CdTe	100	120	Orthorhombic	410941
23.63	CdTe	95.71570	111	Cubic	150770
27.17	ZnTe	93.44693	101	Hexagonal	830967
38.93	Te	86.66015	012	Hexagonal	850563
40.04	CdZnTe	95.91042	220	Cubic/ Rhomboh edral	471296 (Rhomb ohedral)
42.62	CdTe	82.37584	014	Hexagonal	820474
46.34	ZnTe	75.55988	014	Hexagonal	830966
52.67	Te	70.69133	021	Hexagonal	850563
57.92	CdZnTe	70.00975	400/404	Cubic/ Rhomboh edral	471296 (Rhomb ohedral)

Table 4: Un-Annealed Sample

Observed Angle (Degree)	Compound/Element	Observed Intensity (I/Io)	Observed Plane	Crystal Structure	JCPDS File No.
21.3	CdTe	100	120	Orthorhombic	410941
23.6	CdTe	95.65469	111	Cubic	150770
27.15	ZnTe	91.30943	101	Hexagonal	830967
29.2	CdTe	88.52839	102	Hexagonal	800088
35.25	ZnTe	84.12513	102	Hexagonal	800009
42.7	CdTe	72.53766	014	Hexagonal	820474
46.7	ZnTe	66.16454	014	Hexagonal	830966
52.4	CdTe	59.44381	022	Hexagonal	820474
56.2	ZnTe	60.71841	202	Hexagonal	800009

Table 5: Observed $Cd_{1-x}Zn_xTe$ Peaks of the Vaccum, Argon and Nitrogen Annealed Samples

Observed $Cd_{1x}Zn_xTe$ Plane (hkl)	Annealing Type	Observed $Cd_{1x}Zn_xTe$ 2θ (Degree)	Standard Cubic JCPDS CdTe Plane (hkl)	Standard Cubic JCPDS CdTe 2θ (Degree)	JCPDS File No. (CdTe)	Standard Cubic JCPDS ZnTe Plane (hkl)	Standard Cubic JCPDS ZnTe 2θ (Degree)	JCPDS File No. (ZnTe)	Standard JCPDS $Cd_{1x}Zn_xTe$ Plane (hkl)	Standard JCPDS $Cd_{1x}Zn_xTe$ 2θ (Degree)	JCPDS File No. $Cd_{1x}Zn_xTe$
111/003	Vacuum, Argon	24.26, 24.25	111	23.757/ 24.027	150770/ 752086	111	25.259/ 25.502	150746/ 800022	003	24.078	471296
220	Nitrogen	40.04	220	39.310/ 39.741	150770/ 752086	220	41.803/ 42.252	150746/ 800022	220	39.907	471296
311/401	Vacuum, Argon	47.45, 47.4	311	46.431/ 46.977	150770/ 752086	311	49.496/ 50.001	150746/ 800022	401	47.111	471296
400/404	Vacuum, Argon, Nitrogen	58.07, 58, 57.92	400	56.817/ 57.461	150770/ 752086	400	60.632/ 61.289	150746/ 800022	404	57.529	471296

Table 6: Lattice Constant of Observed $Cd_{1-x}Zn_xTe$ Peaks of the Vaccum, Argon and Nitrogen Annealed Samples

Annealing Type	CZT Planes (*hkl*)	2θ (Degree)	Lattice Constant 'a' (nm)	Lattice Constant 'a' of Standard Rhombohedral $Cd_{0.78}Zn_{0.22}Te$ (JCPDS) (nm)
Vacuum Annealed	111	24.26	0.634	0.64
	311	47.45		
	400	58.07		
Argon Annealed	111	24.25	0.635	
	311	47.4		
	400	58		
Nitrogen Annealed	220	40.04	0.636	
	400	57.92		

4.2 *UV-Visible Results*

The samples were subjected to PerkinElmer Lambda 25 Spectrophotometer for an UV-Visible optical test. The wavelength was ranged from 200-900 nm and the absorption spectra were obtained. The molar absorption co-efficient i.e. 'α' is obtained from the absorption spectra by using the following expression [15,16].

$$\alpha = \frac{1}{d}\ln\left(\frac{1}{T}\right) \qquad \ldots\ldots\ldots\ldots (3)$$

Here'd' is the total thickness of the net deposited film including both the CdTe and ZnTe layers and 'T' is the observed transmittance. The band-gap energy of the fabricated thin-films were calculated from graphs with Band-Gap-Energy (hυ) as the x-axis (in eV) and the (Band-Gap-Energy/nm)^2 i.e. $(\alpha h\upsilon)^2$ as the y-axis from the analyzed absorption spectra. The following Figures 5, 6, 7 and 8 reflect such results of the vaccum, Argon, Nitrogen and un-annealed samples respectively.

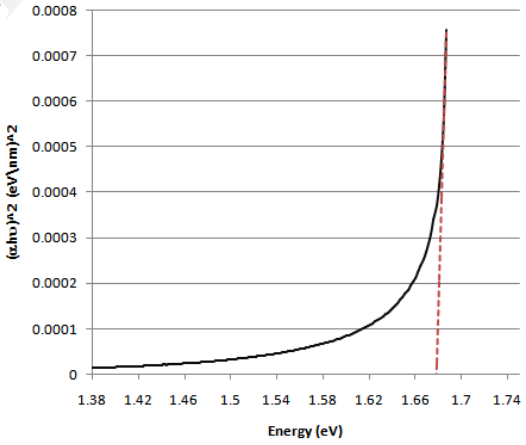

Fig 5: UV-Visible Spectrum of Vaccum Annealed Sample

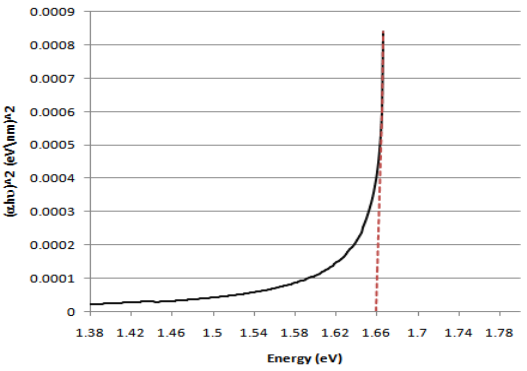

Fig 6: UV-Visible Spectrum of Argon Annealed Sample

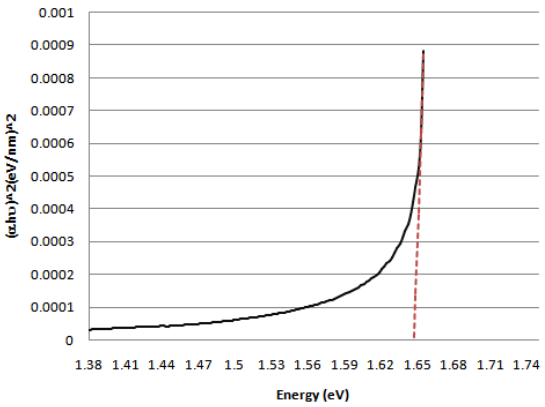

Fig 7: UV-Visible Spectrum of Nitrogen Annealed Sample

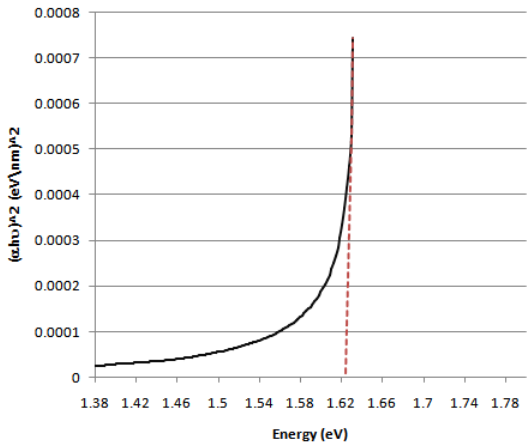

Fig 8: UV-Visible Spectrum of Un-Annealed Sample

Table 7: Band-Gap of Annealed and Un-Annealed Sample

Annealing Type	Approximate Band-Gap (eV)
Vaccum	1.6779
Argon	1.6599
Nitrogen	1.6489
Un-Annealed	1.6251

The band-gap of the annealed samples has an increasing value from the Nitrogen to the vaccum-annealed samples. This result reconfirms the presence of increasing Zinc content in the samples from the Nitrogen to vaccum ones and thus shifts the band-gap energy more from the CdTe side to the ZnTe side. The band-gap of the un-annealed sample is found to have a value lower than all the annealed samples, but is almost in the same band-gap domain. This reflects two things, that the band-gap of the un-annealed sample is dominated both by the individual CdTe and ZnTe layer according to their proportion and lies more close to the CdTe band-gap. This is perhaps because of no loss of Cadmium in the un-annealed sample.

4.3 FTIR Results

Figures 9, 10, 11 and 12 represent the FTIR results of the vaccum, Argon, Nitrogen and un-annealed Sample. The samples were subjected to mid-Infrared rays at room-temperature (300K) by using a Perkin–Elmer FT-IR spectrophotometer model RX-1, lying between 400-4000 cm^{-1} and the transmittance of the sample was plotted on Y-axis. An increasing Tellurium precipitation was observed in the XRD spectrum from the Nitrogen to the vaccum-annealed samples. A predominant trough is observed at around 2660 cm^{-1} in all the annealed-samples with an increasing intensity of the trough from the Nitrogen to the vaccum annealed sample. The above wave-number corresponds to the band-gap of Tellurium i.e. around 0.33 eV and thus indicates the presence of high Tellurium precipitates. Presence of Tellurium precipitate decreases the transmittance or rather increases the absorbance of the infrared rays at its' band-gap or concerned wave-number.

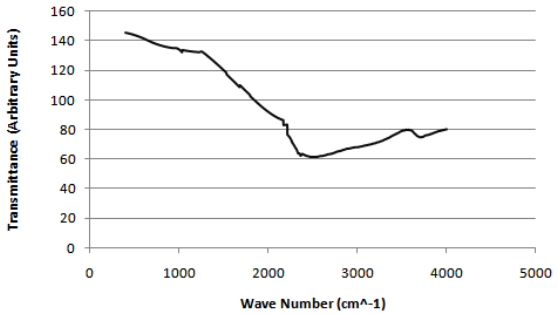

Fig. 9: FTIR Spectrum of Vaccum Annealed Sample

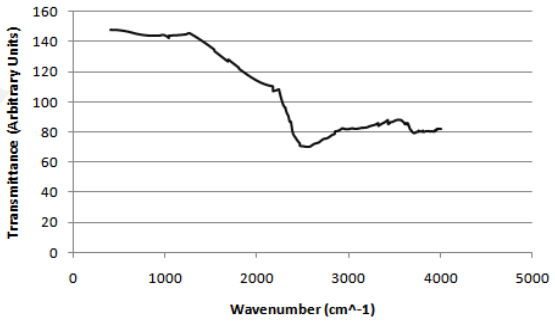

Fig. 10: FTIR Spectrum of Argon-Annealed Sample

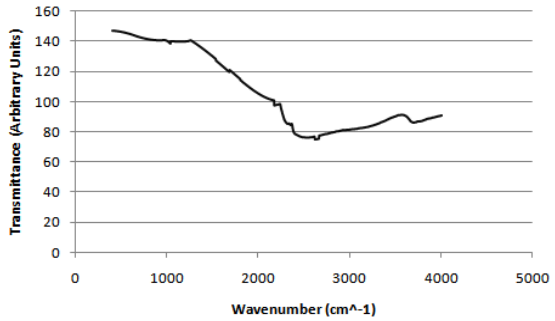

Fig. 11: FTIR Spectrum of Nitrogen Annealed Sample

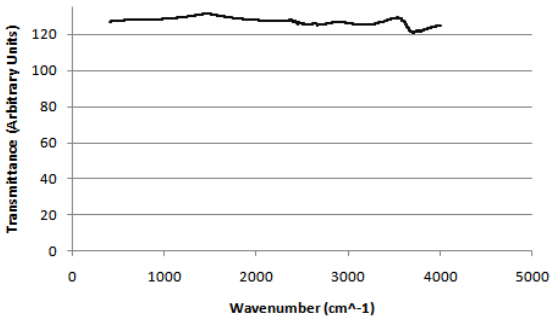

Fig. 12: FTIR Spectrum of Un-Annealed Sample

In case of the un-annealed sample, no such trough or Tellurium presence is observed in the concerned wave-number range as is indicated by the XRD spectrum. The occurrence of the Tellurium planes (in case of XRD) or trough (in case of FTIR) are thus a result of covalent bonding of Cadmium ions of the CdTe to the ZnTe crystal and formation of $Cd_{1-x}Zn_xTe$. This phenomenon is impacted by increasing inertness of annealing environment.

4.4 Photoluminescence Results

Photoluminescence test was carried out on the samples at room temperature (300K) at an excitation of 400nm, at a range of 410-774.5nm, using a Perkin Elmer LS 55 model. For both the vaccum and Argon-Annealed samples, only a single broad banded luminescence is observed at around 1.6666 eV and 1.6489 eV respectively. In this case it should be remembered that obtained band-gap, from the UV-Visible data, of the vaccum and Argon annealed samples were at around 1.6779 and 1.6599 eV respectively. So the energy–gap for transition from the ionized donor bound excitons and from the free excitons level to the conduction band, for the vaccum and Argon-annealed samples is around 11.2 meV and 11 meV respectively. For the Nitrogen annealed sample two photoluminescence peaks are observed; one at 1.6380 eV and another smaller peak at 2.2182 eV. The band-gap for the Nitrogen annealed sample was found at 1.6489 eV. So the first luminescence peak for the Nitrogen annealed sample is because of the energy-transition of the ionized donor bound excitons and neutral donor excitons to the conduction band of the $Cd_{1-x}Zn_xTe$ compound. The second peak is because of the transition of the bound and un-bound excitons to conduction band of the intact ZnTe compound part. It should be noted here that the presence of pure ZnTe peaks were available for the Nitrogen-annealed samples, which was not present for the vacuum and Argon-annealed samples. So the presence of only a single photoluminescence peak in case of the vaccum and Argon-annealed samples is solely because of the transition from bound and unbound excitons to the conduction band of the formed $Cd_{1-x}Zn_xTe$ compound. While for the Nitrogen-annealed sample, the two peaks are for the transition from the bound and unbound exciton to the conduction band of both the formed $Cd_{1-x}Zn_xTe$ and intact ZnTe compound. For the Nitrogen-annealed sample, the energy-gap for the transition from the excitons to the conduction band of the formed $Cd_{1-x}Zn_xTe$ compound is about 10.9 meV. It is found that the energy-gap for this transition from the excitons to the conduction band of the $Cd_{1-x}Zn_xTe$ compound increases from the Nitrogen to the vaccum annealed sample. As the binding-energy of the excitons varies from 10meV from CdTe to about 13 meV in case of ZnTe, it can be inferred here that the increasing Zinc-content of the $Cd_{1-x}Zn_xTe$ compounds from the Nitrogen to the vaccum-annealed samples reflects an increase in binding-energy of the excitons from the Nitrogen to the vaccum-annealed samples. It should be mentioned here that the presence of Tellurium precipitates acts as defects within the annealed samples and leads to formation ionized donor bound excitons and neutral donor bound excitons within those same annealed samples. As proportion of Tellurium precipitates increase from the Nitrogen to vaccum-annealed samples, the intensity of the luminescence because of the transition from excitons (bound and unbound) to conduction band of the $Cd_{1-x}Zn_xTe$ compounds also increases from the Nitrogen to vaccum annealed samples. The un-annealed sample reflects no such major photoluminescence as it has almost zero bound-excitons. A very small peak might be noted at around the band-gap of ZnTe, because of some unbound excitons there. The broadened peaks of the observed luminescence is mostly because of the merging of the phonon replicas at higher temperature. Figures 13, 14, 15 and 16 show the Pl results of the vaccum, Argon, Nitrogen and un-annealed samples.

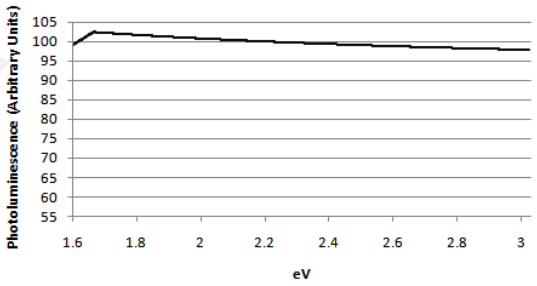

Fig. 13: PL Results of Vaccum-Annealed Sample

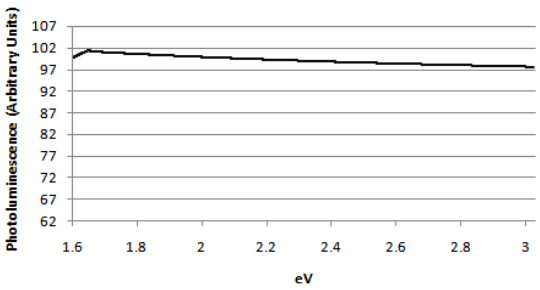

Fig. 14: PL Results of Argon-Annealed Sample

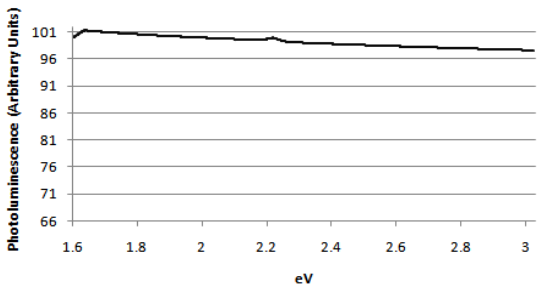

Fig. 15: PL Results of Nitrogen-Annealed Sample

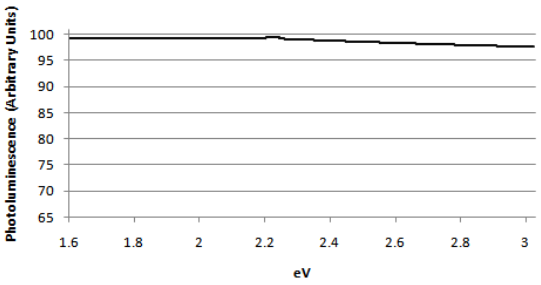

Fig. 16: PL Results of Un-Annealed Sample

4.5 *Strain and Particle Size*

Particle size (L) and strain (ε), in case of polycrystalline structures, is a linear function of FWHM (β) [17] of the observed X-Ray Diffraction peaks and is represented by the following form of the Scherer equation:

$$\frac{\beta cos\theta}{\lambda} = \frac{1}{L} + \frac{\varepsilon sin\theta}{\lambda} \quad \ldots\ldots\ldots\ldots (4)$$

The particle size & strain are retrieved from the intercept and slope of the $(\frac{sin\theta}{\lambda}, \frac{\beta cos\theta}{\lambda})$ graph. The $(\frac{sin\,\theta}{\lambda}, \frac{\beta cos\,\theta}{\lambda})$ plot of the vaccum, Argon, Nitrogen and un-annealed samples are given in Figures 17, 18, 19 and 20 respectively.

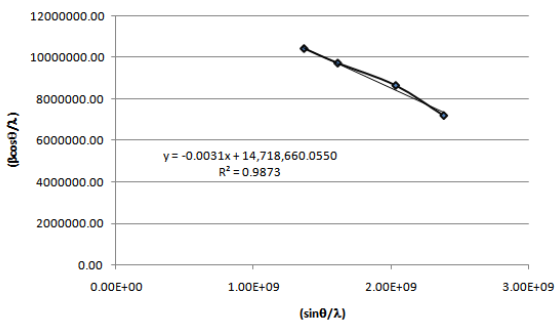

Fig. 17: $(\frac{sin\,\theta}{\lambda}, \frac{\beta cos\,\theta}{\lambda})$ Plot of Vaccum-Annealed Sample

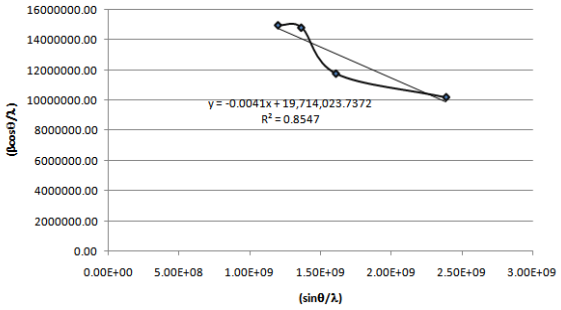

Fig. 18: $(\frac{sin\,\theta}{\lambda}, \frac{\beta cos\,\theta}{\lambda})$ Plot of Argon-Annealed Sample

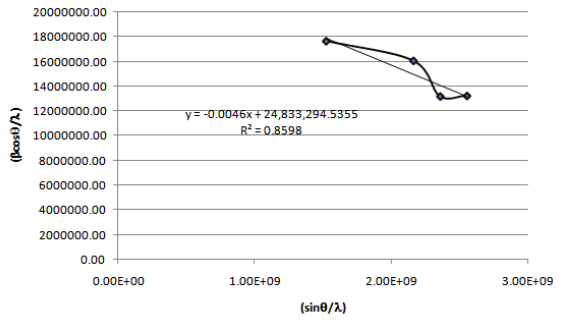

Fig. 19: $(\frac{sin\,\theta}{\lambda}, \frac{\beta cos\,\theta}{\lambda})$ Plot of Nitrogen-Annealed Sample

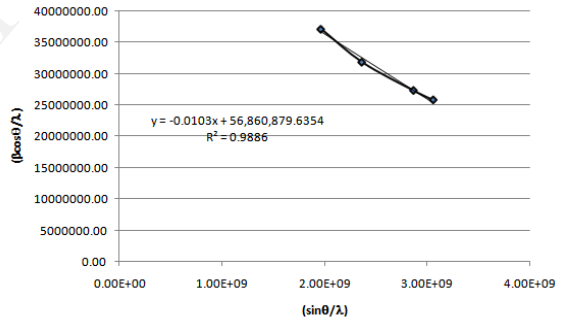

Fig. 20: $(\frac{sin\,\theta}{\lambda}, \frac{\beta cos\,\theta}{\lambda})$ Plot of Un-Annealed Sample

Table 8: Particle size and Strain of Vaccum, Argon, Nitrogen and Un-Annealed Samples

Annealing Type	Particle Size (nm)	Strain
Vaccum	67.94	-0.0031
Argon	50.72	-0.0041
Nitrogen	40.26	-0.0046
Un-Annealed	17.58	-0.0103

A comparative study of the particle size and strain of the samples under various annealing and un-annealed conditions is given Table 8. It is observed there, that a gradual increase in particle size has taken place from the un-annealed to the vaccum-annealed condition. This is also substantiated by the fact from the XRD data, where general XRD peaks of increasing intensities are observed from the un-annealed to the vaccum-annealed samples. As higher

intensity of XRD peaks is a function of more number of inter-lattice planes within the concerned particle, causing more constructive interference, and thus bigger particle size. It can be inferred from the particle size data, that the samples have a generally moved from a polycrystalline structure to a more mono-crystalline structure from the un-annealed to the vaccum-annealed samples. A similar decrease in value of compressive strain is obtained from the vaccum to the un-annealed samples, also implying that a tendency for mono-crystalline structure increases from un-annealed to the vacuum-annealed samples. Figure 21 shows the plot of (Particle Size, Strain) graph, taking values from all the samples.

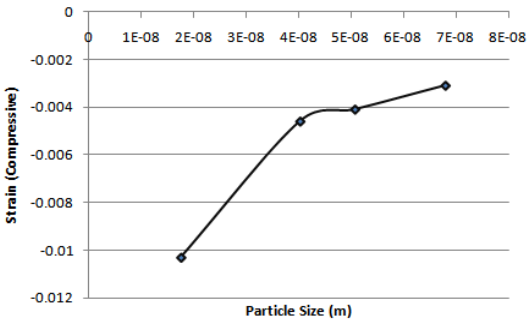

Fig. 21: Strain vs. Particle Size

5. CONCLUSION

The formation of $Cd_{1-x}Zn_xTe$ is associated with more intense Tellurium precipitation in case of layer by layer deposition of CdTe and ZnTe and subsequent annealing. The increased Tellurium precipitation has a direct proportionality effect to the more intense formation of $Cd_{1-x}Zn_xTe$ peaks in the XRD data, as is observed from the Nitrogen to the vaccum annealed samples. Increased inertness of the annealing environment caused quicker heat conduction between the consecutive CdTe and ZnTe layers and improved bonding of the Cadmium ions with the ZnTe crystals and better CZT formation. But the CZT bonds being weaker than their CdTe and ZnTe counterparts, also lead to relative quicker evaporation of the Cadmium from the CZT compound from the vaccum to the Nitrogen annealed samples, curtsy again to the comparative inertness of the environment. This inference is established by the comparison of the lattice-constants of the CZT peaks under the individual annealing environment and that of their band-gap values from the UV-Visible data. Nevertheless, increased Tellurium precipitation initially is always accompanied by better CZT peak formation and is substantiated by the XRD data. Secondly, the increased Tellurium precipitation caused substantial change in the transmittance property of the sample at the band-gap-region of Tellurium and also increased their photoluminescence intensity correspondingly from the Nitrogen to the vaccum-annealed samples, relative to the proportion of Tellurium precipitation in each case. In this regard, the increase of the ionized donor bound excitons and that of the neutral donor bound excitons has caused a relative increase of this particular PL intensity from the Nitrogen to the vaccum-annealed samples, just below the band-gap of the concerned stoichiometric $Cd_{1-x}Zn_xTe$ sample. Lastly, a possible selective formation of the 220 hkl plane of CZT takes place in case of the Nitrogen-annealed sample, rather than the 111 (003) and 311(401) planes as in case of vaccum and Argon annealed sample. As the actual 220 plane in case of cubic CdTe or ZnTe or in case of standard rhombohedral JCPDS $Cd_{0.78}Zn_{0.22}Te$ occurs in between the 111(003) and 311(401) plane, the 220 CZT plane here might have been formed at the cost of the other two 111(003) and 311(401) planes.

ACKNOWLEDGEMENT

Authors are very much thankful to University Grants Commission, Government of India, for providing financial support for this work.

REFERENCES

[1] Peng, H. Olcott, P. D. Pratx, G. Foudray, A. M. K. Chinn, G. and Levin, C. S. 'Design Study of a High Resolution Breast-Dedicated PET System Built from Cadmium Zinc Telluride Detectors', IEEE Nuclear Science Symposium and Medical Imaging Conf., pp 3700-3704 (2007).

[2] Brzymialkiewicz, C. N. Tornai, M. P. McKinley, R. L. and Bowsher, J. E 'Evaluation of fully 3-D emission mammotomography with a compact cadmium zinc telluride detector', IEEE Transactions on Medical Imaging, **24**(7), pp 868-77 (2005).

[3] Krishna, R. M. Muzykov, P. G. and Mandal, K. C. Electron beam induced current imaging of dislocations in Cd0.9Zn0.1Te crystal', J. Physics and Chemistry of Solids, **74**(1), pp 170–173(2013).

[4] Min, J. Chen, J. Liang, X. Zhang, J. Wang, D. and Li, H. 'Effects of gradient heat treatment on Te-rich CdZnTe crystal', J. Vacuum, **86**(7), pp 994-997 (2012).

[5] Willardson, R. K. and Beer, A. C. 'Semiconductors and Semimetals', **13**, Academic, New York, (1978).

[6] Zeng, D. Jie, W. Wang, T. Li, W. and Zhang, J. 'The relationship between stress and photoluminescence of $Cd_{0.96}Zn_{0.04}Te$ single crystal', J. Materials Science and Engineering B, **142**(2-3), pp 144–147(2007).

[7] Faurie, J. P. Reno, J. and Boukerche, M. 'II-VI semiconductor compounds - New superlattice systems for the future?', J. Crystal Growth, **72**, pp 111-116 (1985).

[8] Schlesinger, T. E. and James, R. B. 'Semiconductors and Semimetals', 43rd Edn., Academic, San Diego, (1995).

[9] Dornhaus, R. Nimitz, G. Höhler, G E. and Nickisch, A. 'Narrow-Gap Semiconductors', **98,** Springer, Berlin, (1983).

[10] Shi, Z. Q. Stahle, C. M. Shu, P. 'Fabrication of high-performance CdZnTe strip detector arrays', Proc. SPIE **3553**, pp 90-96 (1998).

[11] Prabakar, K. Venkatachalam, S. Jeyachandran, Y. L. Narayandass, Sa. K. and Mangalaraj, D. 'Microstructure, Raman and optical studies on $Cd_{0.6}Zn_{0.4}Te$ thin films' J. Materials Science and Engineering B,**107**(1), pp 99–105 (2004).

[12] Gadupati,J.'http://etd.fcla.edu/SF/SFE0000341/ThesisCZT.pdf', Master of Science Thesis, University of South Florida, Florida, USA, 2004.

[13] Becerril, M. Silva-Lope, H. and Zelaya-Angel, O. 'Band gap energy in Zn-rich $Zn_{1-x}Cd_xTe$ thin films grown by r.f. sputtering', Revista Mexicana De Fisica, **50** (6), pp588–593 (2004).

[14] Chakraborty, M. 'Optimum Stoichiometry of Cadmium Zinc Telluride Thin Films in the light of Optical, Structural and Photon Generated Studies', Int. J. of Engineering Science and Technology, **3**(4), pp 3799-3806 (2011).

[15] Joshi, G. P Saxena, N. S. Mangal, R. Mishra, A. and Sharma, T. P. 'Band gap determination of Ni—Zn ferrites', Bull. Material Science, **26 (4)**, pp387-389 (2003).

[16] Schlesinger, T. E. Toney, J. E. Yoon, H. Lee, E. Y. Brunett, B. A. Franks, L. and James, R. B. 'Cadmium zinc telluride and its use as a nuclear radiation detector material', Material Science and Engineering, **32**(4-5) (pp 103-189 (2001).

[17] Quadri, S. B. Skelton, E. F. Hsu, D. Dinsmore, A. D. Yang, J. Gray, H. F. and Ratna, B. R. 'Size-induced transition-temperature reduction in nanoparticles of ZnS', Physical Review B, **60** (9191), (1999).